Supersonic Axisymmetric Minimum Length Nozzle Conception at High Temperature with Application for Air

Toufik Zebbiche*
Department of Aeronautics, Faculty of Engineering,
University SAAD Dahleb of Blida, B.P. 270, Blida 09000, Algeria

Abstract

When the stagnation temperature of a perfect gas increases, the specific heats and their ratio do not remain constant any more and start to vary with this temperature. The gas remains perfect; its state equation remains always valid, except, it is named in more by calorically imperfect gas. The aim of this work is to trace the profiles of the supersonic axisymmetric Minimum Length Nozzle to have a uniform and parallel flow at the exit section, when the stagnation temperature is taken into account, lower than the dissociation threshold of the molecules, and to have for each exit Mach number and stagnation temperature shape of nozzle. The method of characteristics is used with the algorithm of the second order finite differences method. The form of the nozzle has a point of deflection and an initial angle of expansion. The comparison is made with the calorically perfect gas. The application is for air.

Key Words : Axisymmetric Minimum Length Nozzle, Prandtl Meyer Function, High Temperature, Numerical Integration, Finite Differences Method, Predictor Corrector Algorithm, Interpolation, Stretching Function, Straight Sonic Line, Calorically Imperfect Gas, Pressure Force, Mass of Nozzle, Relative Error

Nomenclature

A	:	Cross section area
a	:	Sound velocity.
C_F	:	Pressure force coefficient.
C_{Mass}	:	Coefficient of the mass of the nozzle.
C_P	:	Specific heats to constant pressure.
C_y	:	Interpolation coefficient of the ordinate y.
C_θ	:	Interpolation coefficient of the parameter θ.
C_T	:	Interpolation coefficient of the temperature T.
C_W	:	Interpolation coefficient of the deviation of the segment of the wall.
C^+	:	Right running characteristic.
C^-	:	Left running characteristic.
Fx	:	Pressure force exerted on the wall of the nozzle.
H	:	Enthalpy.
HT	:	High Temperature.

* Professor
E-mail : z_toufik270169@yahoo.fr

L	:	Length of the nozzle.
M	:	Mach number.
MLN	:	Minimum Length Nozzle.
MOC	:	Method Of Characteristics
N	:	Number of regular downward characteristics.
N_i	:	Number of the inserted downward characteristics.
P	:	Pressure
PG	:	Perfect Gas.
R	:	Gas constant.
T	:	Temperature.
x, y	:	Cartesian components
θ	:	Flow angle deviation
ν	:	Prandtl Meyer function
μ	:	Mach angle
ρ	:	Density.
ε	:	Tolerance of calculation (desired precision)
γ	:	Specific heats ratio
δ	:	Coefficient of the stretching function.
ξ	:	Downward Mach line.
η	:	Right running Mach line.
α	:	Interpolation coefficient of the pressure.
Δx	:	Non-dimensional step on the line BE of the figure 1.

Subscripts

13	:	Average value between the points 1 and 3.
23	:	Average value between the points 2 and 3.
3	:	Value at the point 3.
0	:	Stagnation condition.
$*$	:	Critical condition.
E	:	Exit section.
d	:	Zone of Kernel.
(j)	:	Segment.
j	:	Node.
W	:	Wall.

Superscripts

*	:	Value at the throat, just after the expansion.
K	:	Iteration.
Iso	:	Iso-value curve.

Introduction

The nozzle is a body used to accelerate a supersonic flow to desired Mach number, in order to generate a thrust like result of this acceleration.

Axisymmetric nozzle design with centred expansion using the MOC is presented in this study, by adding the variation effect of the specific heats $C_P(T)$ with the temperature, which is valid when the stagnation temperature of the combustion chamber is high, but lower than the dissociation threshold of the molecules.

The nozzle design is done according to the manner of its use. For the supersonic blower construction, one wishes that the propulsion of the gas gives a uniform and parallel cold flow to the exit, for reason of measurement and conservation of the experiments tools, independently on the length to be minimal or not. But for the rockets and supersonic aircrafts applications, one interest to obtain nozzles' having a smallest possible weight giving in the same time high possible thrust.

The nozzle is divided into two parts such as subsonic and supersonic region. The supersonic portion is independent to the upstream conditions of the sonic line. The subsonic portion is used to give a sonic flow at the throat. In this class, a nozzle giving a uniform and parallel flow at the exit section, named by Minimum Length Nozzle (MLN), is studied. There are two categories according to the sonic line. For the straight sonic line, the wall at the throat generates centred and divergent expansion waves. The second category has a curved sonic line, where the flow inside the nozzle hasn' t a centred Mach lines. This type is named by MLN with curved sonic line. The MLN with straight sonic line is studied in the references [1] and [3]. Reference [6] studied the axisymmetric MLN with straight sonic line. Reference [7] provides the complete analysis of the MLN 2D with curved sonic line. References [6] and [7] present the analysis of the axisymmetric MLN with curved sonic line.

Figure 1 illustrates the general outline of the axisymmetric MLN with straight sonic line and presents the flow field in various areas. The flow between the throat *OA* and the uniform area *BSE* is divided in two categories. For the 2D and axisymmetric flows, the area *OAB*, named by Kernel region, is of a non-simple waves region. The area *ABE* of transition is a simple region, if the flow is 2D, and the solution can be analytically obtained [2]. However, it is of a non-simple region, if the flow is axisymmetric, and the numerical solution is necessary [9].

The triangular area *BSE* is of a uniform flow region having exit Mach number. The wall at the throat is tilted of an angle θ^*.

The application of the MLN with straight sonic line is limited for the gas dynamics [10] and [12], where only the MLN 2D is used. However, for the hypersonic blowers as well as the rocket motors, the axisymmetric nozzle is used. The study in this work is limited for the axisymmetric MLN with straight sonic line.

The works presented in the previous references [1-3], [6-7], [10] and [12] are realized for the perfect gas (PG) model with constant C_P, which are limited for low stagnation temperatures, where one can go up to approximately 1000K for exit Mach numbers not exceed M_E=2.00. In the reality, the specific heats C_P vary with the temperature. For air and up to 3550K, the reference [10] presents this variation. A polynomial interpolation is made to those values in order to find an analytical form [11] and [13]. For applications, a polynomial of 9^{th} degree is used [14-18] and [21-22].

The aim of this work is to add the variation effect of C_P according to the temperature, lower than the threshold of dissociation, on the supersonic nozzle design. The perfect gas is defined in more by calorically imperfect and thermally perfect, or gas at High Temperature (HT). The conservation equations remain unchanged except that for energy. The new relations at high temperature of the thermodynamic ratios are presented in the references [15] and [22] and that for the Prandtl Meyer function is the goal of the references [14], [19] and [21].

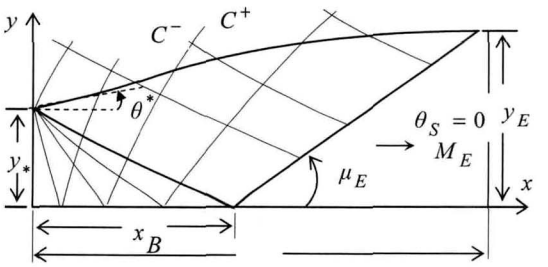

Fig. 1. Flow field inside the axisymmetric MLN

Mathematical formulation

For the axisymmetric supersonic, non rotational, adiabatic flow of a perfect gas, the MOC gives the following equations known by characteristics and compatibilities equations [1] and [18−20]:

Along ξ (1−3), to see figure 2:

$$\begin{aligned} d(v+\theta) &= \frac{\sin\theta \sin\mu}{y} d\xi \\ dy / dx &= tg(\theta-\mu) \end{aligned} \tag{1}$$

Along η (2−3), to see figure 2:

$$\begin{aligned} d(v-\theta) &= \frac{\sin\theta \sin\mu}{y} d\eta \\ dy / dx &= tg(\theta+\mu) \end{aligned} \tag{2}$$

One needs to insert the Prandtl Meyer function in the relations (1) and (2) to obtain a new form valid for HT model which becomes as a generalization of the PG model.
In the relations (1) and (2), the Prandtl Meyer function of the HT model is given by [14], [16−18] and [21]:

$$dv = F_v(T) = -\frac{C_P(T)}{2H(T)} \sqrt{M^2(T)-1}\, dT \tag{3}$$

where [15], [22]

$$M(T) = \frac{\sqrt{2H(T)}}{a(T)} \tag{4}$$

$$a(T) = \sqrt{\gamma(T)\, R\, T} \tag{5}$$

$$\gamma(T) = \frac{C_P(T)}{C_P(T) - R} \tag{6}$$

$$R = 287.102\ J/(kg\ K)$$

The functions $C_P(T)$ and $H(T)$ are presented in the references [15] and [22]. The angle of Mach is given by:

$$\mu = \arcsin(1/M) \tag{7}$$

The relations between the directions of the Mach lines ξ and η and the Cartesian co−ordinates x and y are given by [2]:

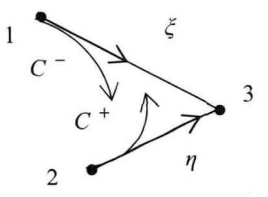

Fig. 2. Characteristic and Mach lines illustration

$$d\xi=\frac{dx}{\cos(\theta-\mu)} \quad , \quad d\eta=\frac{dy}{\sin(\theta+\mu)} \tag{8}$$

Replacing the relations (8) and (3) in the system (1) and (2), one obtains *the following mathematical HT model of MOC*:

Along ξ (1−3):

$$-\frac{C_P(T)}{2H(T)}\sqrt{M^2(T)-1}\,dT+d\theta=\frac{\sin\theta\sin\mu}{y\cos(\theta-\mu)}dx \tag{9}$$

$$dy/dx=tg(\theta-\mu) \tag{10}$$

Along η (2−3):

$$-\frac{C_P(T)}{2H(T)}\sqrt{M^2(T)-1}\,dT-d\theta=\frac{\sin\theta\sin\mu}{y\sin(\theta+\mu)}dy \tag{11}$$

$$dy/dx=tg(\theta+\mu) \tag{12}$$

Where $M(T)$, $a(T)$ and $\mu(T)$ are given respectively by the relations (4), (5) and (7).

As the function $H(T)$ depends on the parameter T_0 [15], [22], the HT model depends primarily on the stagnation temperature T_0 of the combustion chamber.

The developed model is a system of differential equations for four unknowns (x, y, T, θ). The difference between the two models is that, the HT model use the variable T instead M which are connected by an implicit equation (4), where the analytical reverses expression does not exist.

As C^+ and C^- are curved, the application of the MOC obliges us to introduce a fine grid, in order to approximate each characteristic between two points by straight segments. The properties (x, y, T, θ, ρ, P) at the point 3 of the figure 2 can be obtained from those of the points 1 and 2 which connected it. One can make an approximation to the variation of the parameters y, θ and T on the segments connecting the points 1 and 2 and the points 2 and 3 by the following expressions:

$$\theta_{i3}=C_\theta\ \ \theta_i+(1-C_\theta)\ \ \theta_3 \qquad i=1,2 \tag{13}$$

$$T_{i3}=C_T\ \ T_i+(1-C_T)\ \ T_3 \qquad i=1,2 \tag{14}$$

$$y_{i3}=C_y\ \ y_i+(1-C_y)\ \ y_3 \qquad i=1,2 \tag{15}$$

If C_y, C_θ and C_T are chosen equal to 0.5, one obtains the average value of the parameters.

2.1. Equation and procedure for an internal point

Figure 3b presents an internal flow field point. Therefore, the integration of (9), (10), (11) and (12) gives:

Along ξ (1−3):

$$A_{13}\ (T_3-T_1)+(\theta_3-\theta_1)=B_{13}\ (x_3-x_1) \tag{16}$$

$$y_3-y_1=C_{13}\ (x_3-x_1) \tag{17}$$

Along η (2−3):

$$A_{23}\ (T_3-T_2)-(\theta_3-\theta_2)=B_{23}\ (y_3-y_2) \tag{18}$$

$$y_3 - y_2 = C_{23}\ (x_3 - x_2) \tag{19}$$

Where

$$A_{i3} = -\frac{C_P(T_{i3})}{2\,H(T_{i3})}\sqrt{M_{i3}^2 - 1} \qquad i=1,\ 2 \tag{20}$$

$$B_{13} = \frac{\sin(\theta_{13})\,\sin(\mu_{13})}{y_{13}\,\cos(\theta_{13} - \mu_{13})}\ ,\ B_{23} = \frac{\sin(\theta_{23})\,\sin(\mu_{23})}{y_{23}\,\sin(\theta_{23} + \mu_{23})} \tag{21}$$

$$C_{13} = tg(\theta_{13} - \mu_{13})\ ,\ C_{23} = tg(\theta_{23} + \mu_{23}) \tag{22}$$

$$\mu_{i3} = \arcsin(1/M_{i3}) \qquad i=1,\ 2 \tag{23}$$

$$M_{i3} = \frac{\sqrt{2\,H(T_{i3})}}{a_{i3}} \qquad i=1,\ 2 \tag{24}$$

$$a_{i3} = \sqrt{\gamma_{i3}\,R\,T_{i3}} \qquad i=1,\ 2 \tag{25}$$

$$\gamma_{i3} = \frac{C_P(T_{i3})}{C_P(T_{i3}) - R} \qquad i=1,\ 2 \tag{26}$$

Equations (16), (17), (18) and (19) constitute a system of nonlinear algebraic equations of four unknowns (x_3 y_3, T_3, θ_3). The successive iterations algorithm is written:

$$x_3 = \frac{E_2 - E_1}{C_{13} - C_{23}} \tag{27}$$

$$y_3 = E_1 + C_{13}\,x_3 \tag{28}$$

$$T_3 = \frac{D_1 + D_2 + B_{23}\,y_3 + B_{13}\,x_3}{A_{13} + A_{23}} \tag{29}$$

$$\theta_3 = D_1 + B_{13}\,x_3 - A_{13}\,T_3 \tag{30}$$

Where:

$$E_i = y_i - C_{i3}\,x_i \qquad i=1,\ 2 \tag{31}$$

$$D_1 = \theta_1 + A_{13}\,T_1 - B_{13}\,x_1\ ,\ D_2 = -\theta_2 - B_{23}\,y_2 + A_{23}\,T_2 \tag{32}$$

Relations (27) to (30) constitute a system of equations for the calculation at high temperature of internal supersonic flow point properties. The solution is done by the predictor corrector algorithm [3], [9], [11] and [17]. For the predictor step (iteration K=0), the initial values of y_{i3}, T_{i3} and θ_{i3} (i=1,2) are given by:

$$T_{13} = T_1\ ,\ \theta_{13} = \theta_1\ ,\ y_{13} = y_1 \tag{33}$$

$$T_{23} = T_2\ ,\ \theta_{23} = \theta_2\ ,\ y_{23} = y_2 \tag{34}$$

Let us substitute the equations (33) and (34) into equations (27) to (30) to obtain the predicted values $(x_3^0, y_3^0, T_3^0, \theta_3^0)$ as in point 3.

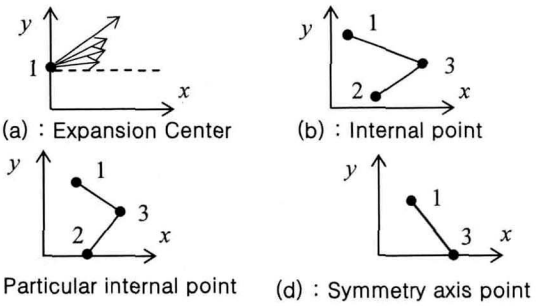

Fig. 3. Different points of calculation

For the corrector algorithm, the values given by the relations (13), (14) and (15) are substituted in equations (27) to (30) to obtain the new values of the parameters as in point 3. The corrected values are $(x_3^1, y_3^1, T_3^1, \theta_3^1)$.

The corrector algorithm must be repeated until having the desired precision. For K iterations, it is necessary to satisfy the following condition to ensure the convergence:

$$\text{Max}\left[\left|y_3^K - y_3^{K-1}\right|, \left|\theta_3^K - \theta_3^{K-1}\right|, \left|T_3^K - T_3^{K-1}\right|\right] < \varepsilon \tag{35}$$

The variable x converge automatically with the convergence of the condition (35)

2.2. Particular internal point

The point 3 of the figure 3c is a particular internal point because the point 2 is on the symmetry axis. The use of the internal point algorithm gives a problem on the calculation of their properties. The term B_{23} in the relation (21) is not defined for the predicted value, since, at the point 2, we have $y_2 = \theta_2 = 0$. As the segment of the Mach line is small, the point 3 will be closer to the horizontal axis. Since one can approaches the nominator of the term B_{23} by $\sin(\theta_{23}) \approx \theta_3$ and the denominator by $\sin(\theta_{23}+\mu_{23}) \approx \sin(\mu_{23})$. The term B_{23} is simplified to:

$$B_{23} \approx \frac{\theta_3}{y_3} \tag{36}$$

Equation (18) remain not valid any more, and will be replaced by:

$$A_{23}\,(T_3 - T_2) - (\theta_3 - \theta_2) = \theta_3 \tag{37}$$

The resolution of equation (37) gives:

$$\theta_3 = \frac{A_{23}\,T_3 - A_{23}\,T_2 + \theta_2}{2} \tag{38}$$

Substituting the equation (38) into relation (16), solution of the obtained equation gives:

$$T_3 = \frac{2\,[D_1 + B_{13}\,x_3) + A_{23}\,T_2]}{2\,A_{13} + A_{23}} \tag{39}$$

Equation (29) must be changed by equation (39). Thus, to determine the properties (x_3, y_3 T_3 θ_3) of this point, one uses the equations (28), (38) and (39) and the iteration procedure is the same as given for regular internal point.

2.3. Equations for the symmetry axis point

As shown in figure 3d, the point 3 is on the axis of symmetry. Because $y_3 = \theta_3 = 0$, the calculation procedure is simplified, and the line ξ joining the points 1 and 3 is employed.

The values of x_3 and T_3 can be obtained by solving the algebraic equations (16) and (17). One obtains

$$x_3 = x_1 - \frac{y_1}{C_{13}} \tag{40}$$

$$T_3 = T_1 + \frac{B_{13}\,(x_3 - x_1) + \theta_1}{A_{13}} \tag{41}$$

One can consider this point as an internal point, if the properties at the point 2 are considered as:

$$x_2 = x_1 \quad , \quad y_2 = -y_1 \quad , \quad \theta_2 = -\theta_1 \quad , \quad T_2 = T_1 \tag{42}$$

2.4. Other parameters

The Mach number M_3 can be obtained by replacing $T = T_3$ into relation (4). The density and the pressure ratios can be determined respectively by the following relations [15], [22]:

$$\left(\frac{\rho}{\rho_0}\right)_3 = Exp\left(-\int_{T_3}^{T_0} C_P(T)/a^2(T)\; dT\right) \tag{43}$$

$$\left(\frac{P}{P_0}\right)_3 = \left(\frac{T}{T_0}\right)_3 \left(\frac{\rho}{\rho_0}\right)_3 \tag{44}$$

3. Procedure of calculation in the nozzle

The flow calculation in the nozzle is divided into two regions, named respectively by region of Kernel and of transition.

3.1. Region of Kernel

The flow calculation in the Kernel region starts from the point A with several manners of design. The first possibility consists to make the design on the basis of the initial flow angle deviation θ^*. The number N of the calculated C must be among the data. The exit Mach number corresponding to this angle will be given just after the calculation of the flow in the Kernel region. Reference [3] uses this manner. It should be noted that for the axisymmetric geometry, there is not an analytical relation between M_E and θ^*.

The second possibility is that, the design can be considered on the basis of M_E. The step $\Delta\theta$ must be among the data. The angle θ^* will be given after the flow calculation in the Kernel region. In this case, a problem meets during the calculation, where the figure 5 presents it. Let us note that our computer code can make the design on the basis of these two possibilities.

There is infinity of Mach waves which result from the point A and reflect on the axis of symmetry. If the design is done on the basis of θ^*, the calculation obliges us to make discretization of the flow expansion zone $0 \leq \theta \leq \theta^*$ in a finite number N of point. In total, one obtains $N+1$ C including the two ends. Then, between two successive characteristics, one chooses:

$$\Delta\theta = \Delta\nu = \frac{\theta^*}{N} \tag{45}$$

If the design is done on the basis of M_E, the calculation obliges us to consider a step $\Delta\theta = \Delta\nu$ rather small. For each passage to a next C, one increment the flow angle deviation at point A by a step $\Delta\theta$ The number of the calculated C is unknown and depends primarily on the chosen step $\Delta\theta$ and on the values of M_E and T_0. The step $\Delta\theta$g=obtained by this manner gives a uniform grid for the C^- of the *end* of the Kernel region, and a large space and non uniform

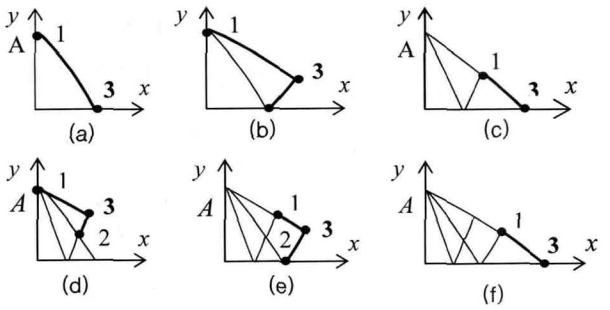

Fig. 4. Calculation process of C^- in the Kernel region

grid for the first C^-. The wall contour just after the throat will be badly presented. To correct this problem, the grid is refined by the insertion of additional C^- between the sonic line and the first C^-. The distribution of the inserted characteristics is carried out by introducing the following grid compression [3] and [17]:

$$\nu_i = \left(\frac{i}{N_i}\right)^{\delta} \Delta\nu \qquad i=1,2,3,4,\ldots,N_i \tag{46}$$

The calculation process in the Kernel region is presented in figure 4. Firstly one determines the properties at the point 1 of the figure 4a. At this point, one have $x_1 / y_* = 0$, $y_1 / y_* = 1$ (non-dimensional). The angle $\theta_1 = \nu_1$ by using the relation (46) if one chooses a grid with compression and $\theta_1 = \Delta\theta$ when the calculation is without procedure of compression. The temperature T_1 must be given by solving the following equation [17]:

$$\theta_1 = \int_{T_1}^{T_*} F_v(T)\, dT \tag{47}$$

Starting from the third C, each one contains 4 types of points. The first type is the point 1 confounded with point A. The second type is the point 3 on the axis of symmetry as the figure 5f showed it. The third one is the particular internal point 3 as shown in the figure 5e and the remainders are of regular internal point. Each type requires a different procedure from the other. Let us note here that the C^- of number i (i=1, 2, 3$\cdots$,N) contains i+1 points. If the Kernel region contains N characteristics, then the total number N_T of points to calculate their properties is exactly equal to:

$$N_T = 2+3+4+\ldots+N = \frac{N(N+1)}{2} - 1 \tag{48}$$

The flow calculation in the Kernel region stops according to the manner of design. If the design is made on the basis of θ^*, the process stops if the calculation for all N selected C^- is completed. The exits Mach number is given as the Mach number of the last calculated point on the axis of symmetry. The properties at this point are those of the exit section. In this case no problem arises, and the end of calculation is done in a normal way as figure 5b shows it. But if the design is made on the basis of M_E, each time that one determines the properties at the points of C^-, one controls if the Mach number M_3 *of* the symmetry axis is equal or just higher than M_E to stop the calculation. In general, a problem is encountered because it is impossible to find $M_3 = M_E$. This problem consists to detect the characteristic C^- containing the Mach number M_E on the axis of symmetry with a precision ε. This situation is presented on the figure 5a. The algorithm of dichotomy [5] and [11] will be used to insert and eliminate C^- between the last two regular C^- (A_2B_2 and A_1B_1), with application of the following relation:

$$M_{B_1} < M_E < M_{B_2} \tag{49}$$

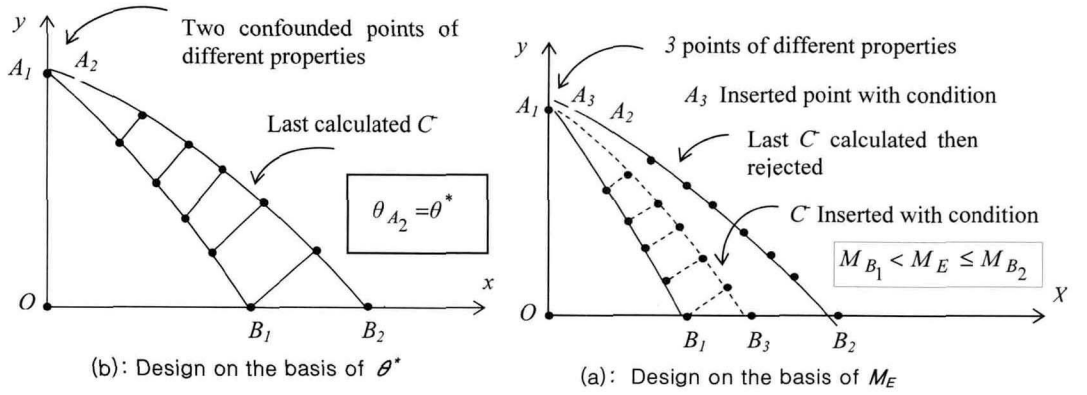

Fig. 5. Different manner of design

A characteristic $(A_3\ B_3)$ will be inserted between the A_1B_1 and A_2B_2, which replaces the rejected A_2B_2. Initially, one inserts a point A_3 with the following condition:

$$\theta_{A_3} = \theta_1 = \frac{\theta_{A_1} + \theta_{A_2}}{2} \tag{50}$$

The temperature T_{A_3} can be determined as solution of equation (47), by substitution of the expression (50) in it, and then on can calculates the properties in all the points of C^- (A_3B_3) up to the point B_3, and checks the condition (49). The calculation will be repeated until one determines the value of M_E with a desired precision ε. The total number of treated C^- will be slightly increased compared to that determined (or given) before the application of the dichotomy algorithm in this particular region.

After the determination of the flow field in the Kernel region, one can determine its length by:

$$\frac{L_d}{y_*} = \frac{x_B}{y_*} \tag{51}$$

3.2. Region of Transition and nozzle contour

The determination of the wall contour in the transition region ABE is done at the same time with the flow calculation in the points of intersection of characteristics, see figure 1.

The control of the grid geometry in this region depends on the chosen distance Δx between the selected points on the uniform Mach line BE. The properties at the points on this line are known, and are equal to the values of the uniform flow of the exit section. Figure 6 presents the calculation process in the region of transition. In the first one calculates the properties of the point 3 of figure 6a. The properties of the point 2 are already determined as the properties of the points on the last C^- of the Kernel region. The properties at point 1 are given by:

$$x_1 = x_B + \Delta x\ ,\quad y_1 = \Delta x\, tg(\mu_E)\ ,\quad \theta_1 = 0.0\ ,\quad T_1 = T_E \tag{52}$$

The value of T_E can be determined by resolution of the equation (4) when $T = T_E$ and $M = M_E$.

The properties at the point 3 can be calculated by the use of the internal point procedure. One passes then to the calculation of the properties at the point 3 of the figure 6b on the same C^-. The successive calculations continue along the direction of the arrows shown in Figure 6b until the last point 3 is determined. The first point of the last characteristic is always a point of the wall (already given).

The difficulty arises is to determine a point of the wall which cuts the calculated C^-. Between two characteristics C^-, one can detect several intermediate wall points. The

various possible cases of detection of the wall points are illustrated in the figure 7. In this figure, the segments connecting the points 1 and 3 and the points 2 and 3 as well as the segment of the wall are regarded as straight lines. The properties at the points 1, 2, 3 and W are known. The intersection of the wall with C^- is named by the point P of properties (x^-, y^-, θ^-, T^-), and the intersection with C^+ is named by the point P^+ of properties (x^+, y^+, θ^+, T^+). To find the point of intersection of the wall with C^+ or C^-, one calculates the following value with the initial approximation $\theta^{\pm} = \theta_W$.

$$\Delta y = y_W - y_1 + (x_1 - x_W)\, tg(\varphi) \tag{53}$$

where

$$\varphi = C_W \theta_W + (1 - C_W)\theta^{\pm} \tag{54}$$

and $C_W \in [0,1]$.

If $\Delta y \geq 0$, one is for the situation (a) or (c) of the figure 7. If $\Delta y < 0$, one is for the situation (b) or (d).

One encounters the case (a) if the number of the wall point' s intersection with C^+ between two C^- is zero. At the beginning of the flow calculation in the region of transition, one meets the case (a) or (d). If $\Delta y \geq 0$, one finds an intersection of the wall with the calculated characteristic. It is necessary to save the parameters (x_P, y_P, T_P, θ_P) of the last calculated point like a new wall point, and to pass to the selection of the new C^- as indicates the figure 8. If $\Delta y < 0$, one did not find yet an intersection of the wall with the calculated characteristic. To determine the properties of the new detected point of the wall, one assume a linear variation of θ on the segment connecting the points 1 and 3 if $\Delta y \geq 0$, and on the segment connecting the points 2 and 3 if $\Delta y < 0$, to see figure 7.

1st Case: If $\Delta y \geq 0$

When $\xi = 0$, one has $\theta_{13}(\xi) = \theta_3$ and when $\xi = \Delta \xi_{13}$ (distance between the points 1 and 3) one has $\theta_{13}(\xi) = \theta_1$. The linear variation of the angle θ gives the following result to the point P^-:

$$\theta^- = \theta_3 + \left[\frac{(x^- - x_3)^2 + (y^- - y_3)^2}{(x_3 - x_1)^2 + (y_3 - y_1)^2}\right]^{1/2} (\theta_3 - \theta_1) \tag{55}$$

2nd Case: If $\Delta y < 0$

When $\eta = 0$, one has $\theta_{23}(\eta) = \theta_2$ and when $\eta = \Delta \eta_{23}$ (distance between the points 2 and 3), one has $\theta_{23}(\eta) = \theta_3$. The linear variation of the angle θ, gives the following result to the point P^+:

$$\theta^+ = \theta_2 + \left[\frac{(x^+ - x_2)^2 + (y^+ - y_2)^2}{(x_3 - x_2)^2 + (y_3 - y_2)^2}\right]^{1/2} (\theta_3 - \theta_2) \tag{56}$$

The determination of the position of the point P^- is done by writing the equations connecting the points 1 and 3 and the points W and P. For the determination of the position of the point P^+ by one write the equations connecting the points 2 and 3 and the points W and P^+. One obtains:

$$x^{\pm} = \frac{y_3 - y_W - x_3 \lambda^{\pm} + x_W tg(\varphi^{\pm})}{tg(\varphi^{\pm}) - \lambda^{\pm}} \tag{57}$$

$$y^{\pm} = y_3 + \lambda^{\pm} (x^{\pm} - x_3) \tag{58}$$

Where

$$\varphi^{\pm} = C_W\ \theta_W + (1-C_W)\ \theta^{\pm} \tag{59}$$

$$\lambda^{+} = \frac{y_3 - y_2}{x_3 - x_2} \quad , \quad \lambda^{-} = \frac{y_3 - y_1}{x_3 - x_1} \tag{60}$$

The relation (57) represent a nonlinear algebraic equation used for the determination of the position (x^-, y^-) of the point P^- and the position (x^+, y^+) of the point P^+. Initially, one assumes the angle $\theta^{\pm} = \theta_W$. By substitution of this approximation into (57) and (58), we can obtain the initial approximation of the position of $P^{\pm}$. This value must be substituted in the relation (55) to correct the angle θ^-, or in the equation (56) to correct the angle θ^+. The procedure will be repeated until satisfying the convergence criterion (61).

$$\mathrm{Max}\left[\left| x^{\pm}(K) - x^{\pm}(K-1)\right| , \left| y^{\pm}(K) - y^{\pm}(K-1)\right|\right] < \varepsilon \tag{61}$$

Between each two successive iterations, it is necessary to check the condition (53) for the new corrected value of θ^- or θ^+ to take the necessary equation between the point P^+ or P^-, for aim to detect exactly the point of the wall. Once the position of the wall position is determined, it will be regarded as a new point of the wall, and one or two of the configurations of figure 7 were applied. The procedure will be repeated for the next selected C^- in the region of transition. The presentation of the wall depends on the selected step Δx for the points of the uniform Mach line BE and on the obtained properties on the last C of the Kernel region.

Once the position of the points P^+ or P^- is determined, the deviation angle of the wall converges at the same time with the computing process, and the temperature in these points can be calculated by supposing a linear variation of it on the segments connecting the points 1 and 3 and the points 2 and 3 with the same step as the angle θ. The temperature is interpolated respectively for the point P^- and P^+ as:

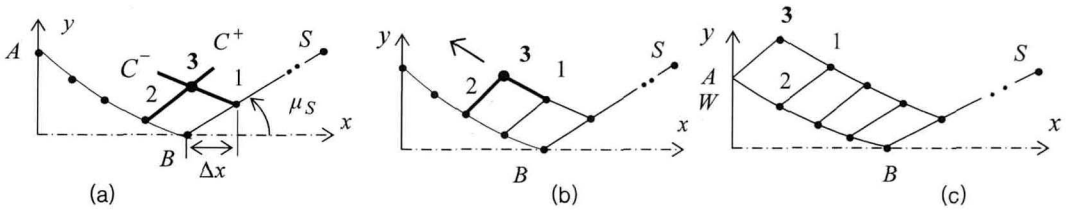

Fig. 6. Computing process of the C^- in the transition region

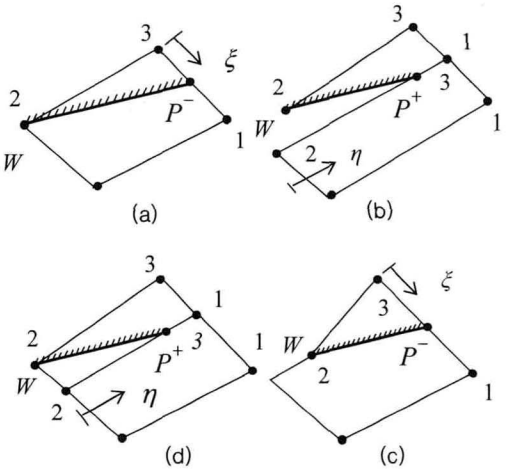

Fig. 7. Different cases of intersection of the wall with characteristics

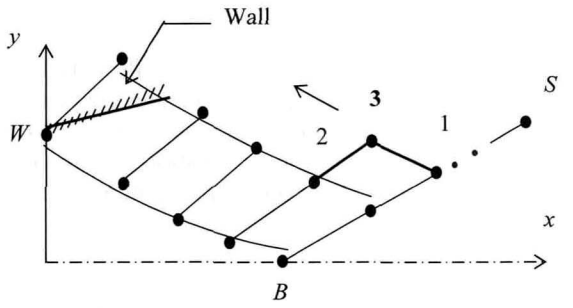

Fig. 8. Passage from characteristic to another in the region of transition

$$T^{-}=T_3+\left[\frac{(x^{-}-x_3)^2+(y^{-}-y_3)^2}{(x_3-x_1)^2+(y_3-y_1)^2}\right]^{1/2}(T_1-T_3) \tag{62}$$

$$T^{+}=T_2+\left[\frac{(x^{+}-x_2)^2+(y^{+}-y_2)^2}{(x_3-x_2)^2+(y_3-y_2)^2}\right]^{1/2}(T_3-T_2) \tag{63}$$

To obtain the Mach number in this point, one replacing the obtained value of the temperature in the equation (4). The thermodynamic ratios can be obtained by replacing the values of T_3 with the obtained value of T^{-} or T^{+} in the relations (43) and (44).

The procedure will be repeated for each selected C^{-} until one determines an intersection of the wall with the uniform characteristic BE. One advances to the exit point on line BE, the number of internal points to be calculated on the corresponding C decreases until to obtain one point. This situation is obtained wants to means that the calculation arrives at the point E of the exit section. Consequently, the non-dimensional exit radius corresponding to the discretization will be given by:

$$\frac{y_E}{y_*}(computed)=\frac{y_{N_W}}{y_*} \tag{64}$$

The number of points found on the nozzle wall (precisely the number N_W in the relation (64)) depends on the selected step Δx on the uniform $C^{-}BE$ and on the number of the points on the last $C^{-}AB$ of the Kernel region. This number is higher or equal to the number of points chosen on the uniform $C^{-}BE$ and even higher than the obtained number of points N_C on the last $C^{-}AB$ of the Kernel region.

$$N_W = f(N_C, \Delta x, \text{provision of points on the } C^{+}BE) \tag{65}$$

Where

$$N_C = f(M_E, T_0, \Delta\theta, N_i, \delta) \tag{66}$$

Which is not the case for the geometry 2D, where the number $N_W=N_C$ [17].

The comparison of the obtained numerical results is made between the numerical calculated ray at the exit section and with the theoretical non-dimensional ratio of the cross sectional area presented by the following formulae [15], [22]:

$$\left(\frac{y_E}{y_*}\right)^2_{Theoretical}=\frac{A_E}{A_*}=\mathrm{Exp}\left(\int_{T_E}^{T_*} F_A(T)\,dT\right) \tag{67}$$

Where $F_A(T)$ is presented in the references [15] and [22].

3.3. Iso-values curves

It is very interesting to determine curves in the flow field, having even constant physical properties. These curves are called by iso-values curves. Most interested are the iso-Mach and the iso-directions curves. The iso-pressures, iso-temperatures and the iso-density curves are the iso-Mach. The determination of the points of these curves is done after the calculation of the internal flow on each segment of characteristics as figure 9 shows it.

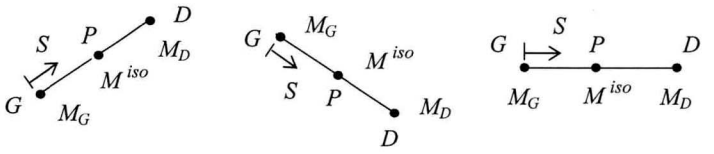

(a) On C^+ and the wall (b) On C^- (c) On the axis of symmetry

Fig. 9. Various segments of points of the iso-Mach curves

The properties (x, y, M, $T\cdots$) in the points G and D are known. The problem becomes the determination of the position (x_P, y_P) of the point P having a given property (M or θ).

Prior to find the properties in the points of C^+, C^-, the axis of symmetry or the wall, one makes the following test:

$$\Delta y = y_D - y_G \tag{68}$$

- If $\Delta y>0$, The point is find on the C^+ or on the wall.
- If $\Delta y<0$, The point is find on the C^-.
- If $\Delta y=0$, The point is find on the symmetry axis.

3.3.1. Iso-Mach curves

Let M^{iso} the value of the Mach number which an internal whole of points in the nozzle must have, that one must determine their positions. The segment containing the point P of the iso-Mach curve must satisfy the following condition:

$$(M^{iso}-M_G)(M^{iso}-M_D)\leq 0 \tag{69}$$

The determination of the position of the point P, requires to consider a linear variation $M(S)=\alpha S+\beta$ of the Mach number on the segment GD. When $S=0$, one has $M(S)=M_G$ and when $S=S_{GD}$ (distance between the points G and D), one has $M(S)=M_D$. The relation $M(S)=M_P=M^{iso}$ is checked when $S=S_{GP}$. Then, the distance between the points G and P is given by:

$$S_{GP}=\frac{M^{iso}-M_G}{M_D-M_G}\sqrt{(x_G-x_D)^2+(y_G-y_D)^2} \tag{70}$$

The position (x_P, y_P) of the point P of the iso-Mach curve can be determined by:

$$x_P = x_G + S_{GP}\ \cos(\theta_{GD}) \tag{71}$$

$$y_P = y_G + S_{GP}\ \sin(\theta_{GD}) \tag{72}$$

Where:

$$\theta_{GD} = arctg\left(\frac{y_D - y_G}{x_D - x_G}\right) \tag{73}$$

3.3.2. Iso-direction curves

The determination of the points of the iso-direction curve having $\theta = \theta^{iso}$ is made by the same manner as the iso-Mach curves. The relations (69) and (70) will be changed respectively by:

$$(\theta^{iso} - \theta_G)(\theta^{iso} - \theta_D) \leq 0 \tag{74}$$

$$S_{GP} = S^{iso} = \frac{\theta^{iso} - \theta_G}{\theta_D - \theta_G} \sqrt{(x_G - x_D)^2 + (y_G - y_D)^2} \tag{75}$$

The position (x_P, y_P) of the point P can be determined by the relations (71) and (72), and for the value of θ_{GD}, the relation (73) must be used.

3.4. Mass of the structure of the nozzle

To calculate the mass of the nozzle, one considers the two following assumptions:

1. The shape of the wall between two successive points is approximated by a straight line. This assumption gives good result if the number N_W of points is very high.
2. The structure of the divergent is made up of the same material having a constant thickness t_M and density ρ_M.

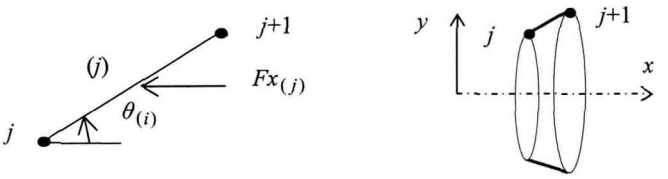

(a): Pressure force (b): Segment of nozzle

Fig. 10. Presentation of a segment of the nozzle

The calculation of the mass of the nozzle depends on the calculation of its area of revolution. As one has $(N_W - 1)$ segments, then, in non-dimensional form, the mass can be obtained by:

$$\frac{Mass}{\rho_M \, t_M \, A_*} = C_{Mass} = \sum_{j=1}^{j=N_W-1} \frac{S_{(j)}}{A_*} \tag{76}$$

Where: $S(j)$ represents the area of revolution of the circular nozzle limited between the points j and $j+1$ $(j=1, 2\cdots, N_W-1)$ as indicated in figure 10. According to the Guldin' s theorem [4], the section area $S_{(j)}$, can be calculated, in the non-dimensional form, by:

$$\frac{S_{(i)}}{A_*} = \left(\frac{y_i}{y_*} + \frac{y_{i+1}}{y_*}\right)\left[\left(\frac{x_{j+1}}{y_*} - \frac{x_j}{y_*}\right)^2 + \left(\frac{y_{j+1}}{y_*} - \frac{y_j}{y_*}\right)^2\right]^{1/2} \tag{77}$$

3.5. Pressure force exerted on the wall of the divergent

To calculate the pressure force exerted on the wall, one considers that the pressure exerted on the section (j) of the figure 10 is approximated by:

$$P_{(j)} = \sigma P_j + (1-\sigma) P_{j+1} \tag{78}$$

For the applications, one takes $\sigma = 0.5$.

Thus, the axial pressure force F_x exerted on the wall is given as the sum of the all axial pressure forces exerted on the all sections of the nozzle. In non-dimensional form, one obtains:

$$\frac{F_x}{P_0 A_*} = C_{Force} = \sum_{j=1}^{j=N_W-1} \left(\frac{P_{(j)}}{P_0}\right)\left(\frac{S_{(j)}}{A_*}\right) \sin(\theta_{(j)}) \tag{79}$$

The pressures ratio in the expression (79) is given by the relation (44) and the angle $\theta_{(j)}$ can be obtained by the following relation:

$$\theta_{(j)} = arctg\left(\frac{y_{j+1} - y_j}{x_{j+1} - x_j}\right) \tag{80}$$

In the relations (77) and (79), the value of A_* is equal to πy_*^2.

4. Error given by the perfect gas model

A comparison between the results given by the two models will be made. For each values of (T_0, M_E), the error given by the PG model compared to the HT model can be calculated for each design parameter by the following relation:

$$\varepsilon_{Parameter}\,\% = \left| 1 - \frac{Parameter_{PG}}{Parameter_{HT}} \right| \times 100 \tag{81}$$

The word parameter in the relation (81) represents all design parameters, in particular, the length of the nozzle, the mass of the structure, the pressure force and the critical cross sectional ratio.

5. Results and comments

5.1. Grid in characteristics

Figures 11 to 14 present the grids in characteristics in each flow region by the exploitation of the various parameters intervening on the grid generation. Each parameter has an importance which goes influences the results of design. The nature of a supersonic flow depends on the upstream condition. Then an error at the beginning of calculation (throat) will be propagated in order to be rather large at the exit section, without forgetting the errors caused by the computing mathematical operations, that one call by artificial viscosity. The selected example is for T_0=2000K, M_E=3.00 which gives θ^*=13.08 degree. Physically the flow field necessary for calculation is divided into two parts, that of Kernel and the transition region, but mathematically and numerically one divides it by four parts, of Kernel, of transition, zone of insertion of additional C^- between the first regular C^- regular and the sonic line. For each area there is a parameter which interprets the obtained grid. Each area is the goal of a figure among the four presented.

In figure 11 one presents the grids refinement of the zone of transition by the variation of the non-dimensional step Δx, without variation of the other parameters. The numerical results are presented in table 1. It is clear to examine the obtained error on the exit ray. The progression of the error is not honoured, for reason that the error given by the three others areas influenced the results in this area, and consequently on the design results. One can obtain results with an error 10^{-5}, if one refines at the same time the grid in the other areas. The values of N_C, θ^*, M^* and the length of Kernel do not depend on the discretization of the zone of transition. They depend primarily on $\Delta\theta$, N_i and δ. for the suggested example, the obtained values are respectively equal to N_C=139, θ^*=13.135 degree, M^*=1.513 and L_d/y_*=2.7361.

In figure 12 one refined the grid in the zone of Kernel without insertion of additional C^-. The example (a) of this figure is that of the case (b) of the figure 11. Let us decrease the step $\Delta\theta$, one can obtain other configurations, where three examples are presented on the cases (b), (c) and (d). The obtained numerical results of design are presented in the table 2.

Here, all the parameters depends on the step $\Delta\theta$. The examination of the obtained error on the exit ray, the refinement in this area can decrease the error. One can go to 0.03%, if $\Delta\theta$ =0.005 degree is selected. If one mixes the case (d) of the figures 11 and 12, one can obtain an error $\varepsilon=10^{-5}$.

Figure 13 presents some grids with insertion of additional C^- for $\delta=2$. The case (a) of this figure is that of the case (a) of the figure 12 without effect of condensation. In the three others cases (b), (c) and (d), one inserted respectively, $N_i=5$, $N_i=10$ and $N_i=50$ C^-. The obtained numerical results of design are presented in the table 3. In let us examine the obtained error for each values of N_i, one can noticed that, a precision $\varepsilon=10^{-4}$ can be obtained. The results in the Kernel region depend on the obtained results in the region just after the insertion of the additional C^-. One notices that there is progressive closing towards the throat as well as the reduction in the distance between the first C^- (inserted) and the sonic line.

In the figure 14, one presented grids by changing the coefficient δ of the function (46), for goal of good presentation of the wall at the throat. If δ is large, the distance between the sonic line and the first C^- decreases which influences the design results, in particular the presentation of the wall at the throat. The numerical results of design for various values of δ are presented in the table 4. In let us compare the results of table 3 when N=10 and the results in the table 4, one can notice that one can go from an error 10^{-3} to 10^{-4}, which demonstrates the influence of this coefficient on the grid presentation and on the design results.

If one takes in the same time the parameters of the case (d) of each figure, one can obtain approximately an error $\varepsilon=10^{-6}$.

It is noticed that it is very interested to refine the grid on the wall in the vicinity of the throat. In conclusion on figures 11 to 14, one can say that one can design a nozzle with a moderate number of points on the wall if one uses the refinement of the grid by insertion of additional C^-.

The values of N_C and N_W corresponding to the results of the table 4 are equal respectively to 1323 and 1992.

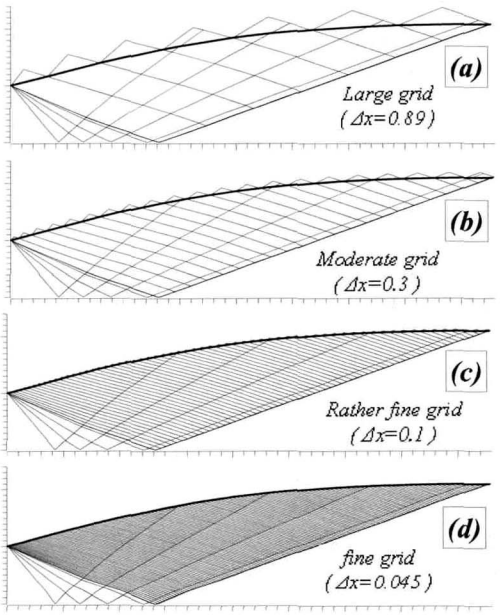

Fig. 11. Grid refinement in the zone of transition transition with $\Delta\theta$=3.0 degree and N_f=0

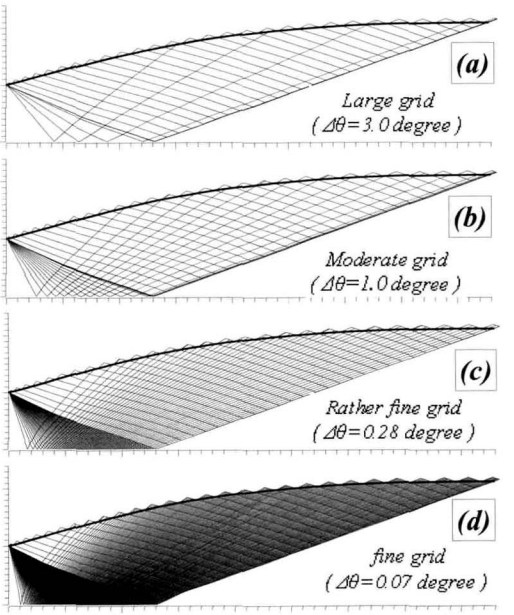

Fig. 12. Grid refinement in the zone of Kernel without insertion of additional C for Δx=0.30

Table 1. Effect of refinement of the transition zone on the design parameters convergence for T_0=2000K, M_E=3.00, $\Delta\theta$=0.1 degree and N_i=0

Δx	N_W	$\frac{y_E}{y_*}$	$\frac{L}{y_*}$	C_{Mass}	C_{Force}	ε (%)
2.0	143	2.20007	8.482	35.523	0.302	3.153
1.0	146	2.22219	8.891	34.682	0.315	1.168
0.7	149	2.22689	8.909	34.815	0.320	0.741
0.5	153	2.22960	8.920	34.893	0.324	0.496
0.3	162	2.23158	8.966	34.782	0.329	0.318
0.1	206	2.23271	9.050	34.462	0.333	0.216
0.07	235	2.23279	9.042	34.501	0.334	0.209
0.05	273	2.23285	9.051	34.467	0.334	0.204
0.03	363	2.23290	9.043	34.504	0.334	0.199
0.01	809	2.23291	9.051	34.469	0.335	0.198

Table 2. Refinement effect of the Kernel zone on the convergence of the design parameters for T_0=2000K, M_E=3.00, Δx=0.05 and N_i=0

$\Delta\theta$ (°)	$\frac{y_E}{y_*}$	$\frac{L}{y_*}$	C_{Mass}	C_{Force}	ε (%)
2.0	2.2153	9.025	34.018	0.287	1.798
1.0	2.2231	9.026	34.271	0.305	1.084
0.7	2.2258	9.034	34.332	0.312	0.832
0.5	2.2279	9.039	34.370	0.318	0.647
0.3	2.2301	9.045	34.415	0.324	0.445
0.1	2.2328	9.051	34.467	0.334	0.204
0.07	2.2333	9.031	34.566	0.336	0.160
0.05	2.2336	9.032	34.573	0.338	0.128
0.03	2.2341	9.032	34.580	0.340	0.092
0.01	2.2346	9.033	34.589	0.343	0.047

Table 3. Effect of the addition of C^- in the Kernel region on the convergence of the design parameters for T_0=2000K, M_E=3.00, $\Delta\theta$=0.01 degree, Δx=0.01 and δ=3

N_i	$\frac{y_E}{y_*}$	$\frac{L}{y_*}$	C_{Mass}	C_{Force}	ε (%)
0	2.2346	9.04997	34.51844	0.3443	0.043
1	2.2346	9.04997	34.51844	0.3443	0.043
2	2.2346	9.04997	34.51844	0.3443	0.043
5	2.2350	9.05014	34.52450	0.3472	$9.1\ 10^{-3}$
10	2.2351	9.05011	34.52541	0.3481	$3.0\ 10^{-3}$
20	2.2351	9.05008	34.52566	0.3486	$1.1\ 10^{-3}$
30	2.2351	9.05008	34.52574	0.3488	$6.9\ 10^{-4}$
50	2.2351	9.05007	34.52574	0.3489	$4.3\ 10^{-4}$

Table 4. Effect of the coefficient δ on the convergence of the design parameters for T_0=2000K, M_E=3.00, $\Delta\theta$=0.01 *degree*, Δx=0.01 and N_i=10

δ	$\frac{y_E}{y_*}$	$\frac{L}{y_*}$	C_{Mass}	C_{Force}	ε (%)
1	2.23494	9.05015	34.52328	0.3465	$1.6\ 10^{-2}$
2	2.23505	9.05014	34.52489	0.3476	$6.6\ 10^{-3}$
3	2.23510	9.05011	34.52541	0.3481	$3.0\ 10^{-3}$
4	2.23511	9.05017	34.52523	0.3484	$1.5\ 10^{-3}$
5	2.23512	9.05019	34.52515	0.3485	$1.0\ 10^{-3}$
6	2.23512	9.05020	34.52510	0.3485	$8.4\ 10^{-4}$
7	2.23512	9.05020	34.52506	0.3485	$8.3\ 10^{-4}$
8	2.23512	9.05020	34.52507	0.3486	$8.1\ 10^{-4}$

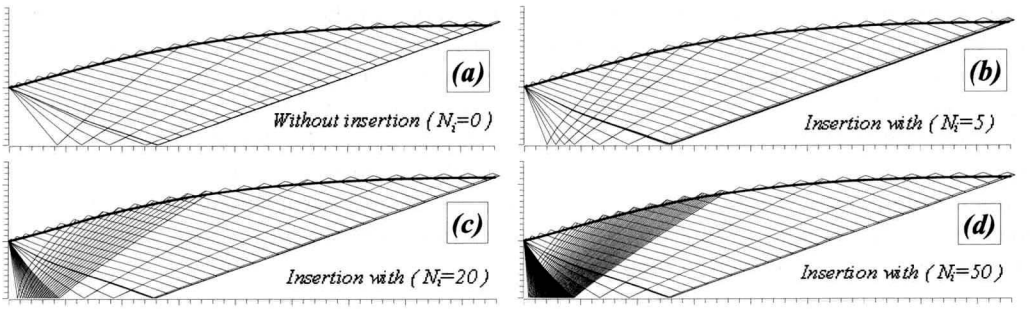

Fig. 13. Insertion of additional C^- in the zone of Kernel for δ=2, $\Delta\theta$=3.0 and Δx=0.23

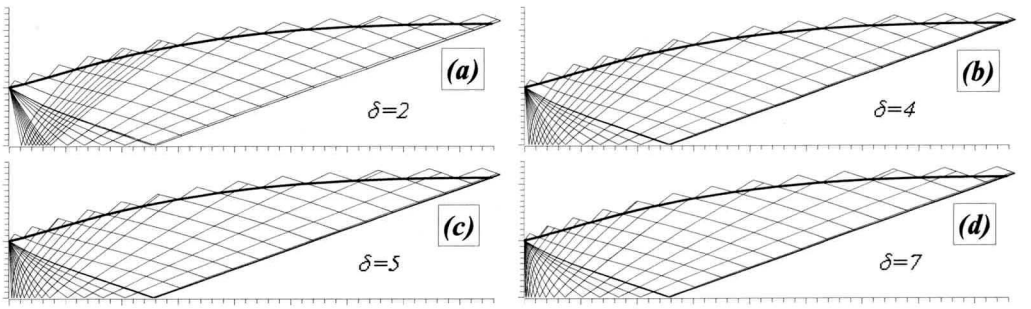

Fig. 14. Effect of the coefficient δ on the grid quality with $\Delta\theta$=2.0 degree, Δx=0.5 and N_i=10

5.2. Effect of T_0 on the wall contour

Figure 15 presents the shapes of the nozzles giving respectively M_E=1.50, 2.00, 3.00, 4.00, 5.00 and 6.00 at the exit section. Each case contains 4 curves, where three of them are for the HT model corresponding to T_0=1000K, 2000K and 3000K, including the case 4 of the PG model for γ=1.402;

According to the obtained forms on the part (a), one notices a very small difference between the four curves.

The part (b) of the figure 15 shows the form of the nozzle when M_E=2.00. One notices that the difference is always small but greater than the error compared to the case (a).

By increasing the exit Mach number, the case (c), (d), (e) and (f) of the figure 15 present respectively the obtained contours for M_E=3.00, 4.00, 5.00 and 6.00.

One can say that if T_0 increases, the difference between the PG and HT models increased and becomes considerable if T_0>1000K independently of M_E, or from M_E>2.00 for any value of T_0. This limit can be found if one chooses an error ε lower than 5%.

Before the tracing of the figure 15, one made a study on the wall discretization by increasing the numbers N, N_i and δ, and each time one determines the design parameters and calculates the relative error given by the non-dimensional exit section ray by using the relation (82) until satisfying an accuracy of 10^{-4}.

$$\varepsilon\left(\frac{y_E}{y_*}\right)(\%)=\left|1-\frac{(y_E/y_*)_{Computed}}{(y_E/y_*)_{Theoretical}}\right|\times 100 \tag{82}$$

The calculated and theoretical ratios y_E/y_* are respectively given by the relations (64) and (67).

It was noticed that the length of Kernel, length of the nozzle, the mass of the structure and the pressure force converge before the convergence of the exit section ray towards the exact solution. This property is an advantage in order to control only the convergence of the exit ray section. The parameters converge by a decreasing way, i.e. the exact solution is always lower than the numerical solution. It is still noticed that this type of nozzle has a deflection point having an angle θ_{max} near to the throat. Then, the deviation angle of the wall increases from θ^* to θ_{max} and then decreases gradually until θ=0 at the exit section. The position of the point of deflection, for some values of M_E and T_0 including the case of the PG model [3] are presented in table 5. The Mach number and the flow angle deviation of the deflection point are presented in table 6.

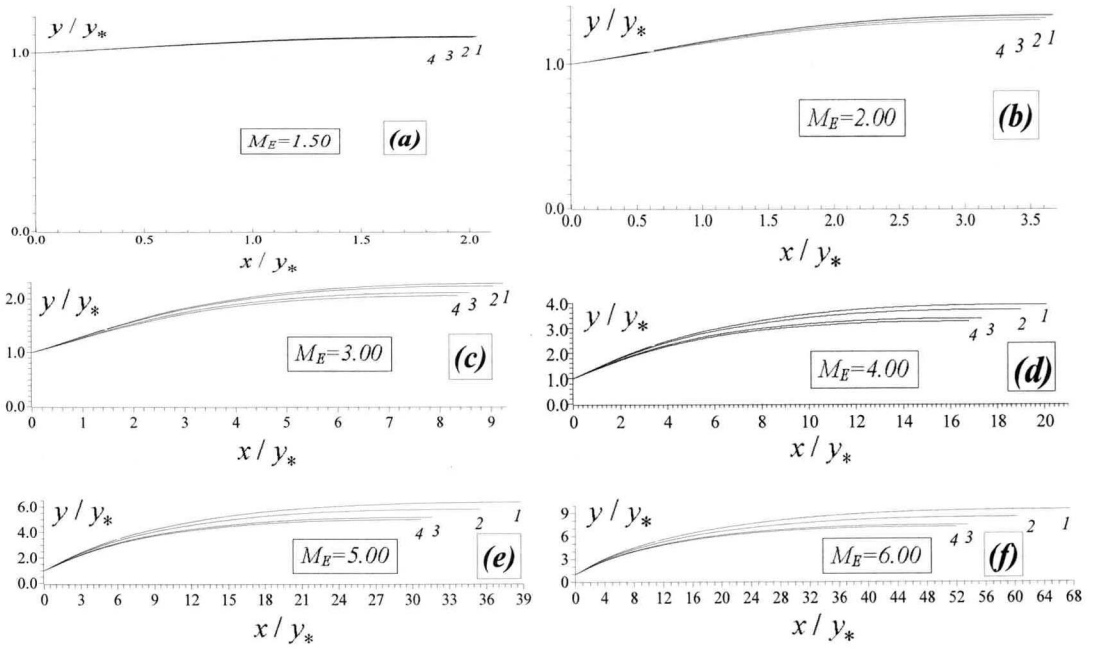

Fig. 15. Shapes of the nozzle giving different exit Mach number M

5.3. Variation of the parameters along the wall

Figures 16, 17 and 18 represent the variation at high temperature of the thermodynamic ratios (T/T_0, ρ/ρ_0, P/P_0) along the wall of the nozzle. One notices a reduction of the parameters through the divergent. The effect of T_0 on these parameters is well presented.

The ratio T/T_0 enables us to make a suitable choice of the building materials which can resist this distribution of temperature and used to us to determine the internal boundary condition to make the study of heat transfer through the materials of the wall.

During the expansion, the gas goes cooled, where the temperature T_* is always higher than T_E. The PG model indicates a cooling compared to the real thermodynamic behavior, especially if T_0 is raised, for example if T_0=2000K, then T_*=1665K and T_E=1108K for the PG model and T_*=1737 K and T_E=1232 K for the HT model. Therefore a difference in 72 K at the throat and 124 K at the exit section is obtained.

The ratio P/P_0 will be used to determine the pressure force exerted on the wall.

The ratio ρ/ρ_0 will be used to determine the quantity of the gas which will cross the divergent, in order to determine the lifespan of the fuel.

Figure 19 represents the variation of the flow angle deviation through the wall of the nozzle. One notices the existence of a deflection point closer to the throat, from where the flow expansion from θ=0 to $\theta=\theta^*$ at the throat (abrupt expansion) then increases to $\theta=\theta_{max}$ at the point of deflection then will to rectified to θ=0 at the nozzle exit. The intersection of the four curves with the vertical axis represents the value of $\theta=\theta^*$. The values of $\theta=\theta_{max}$ are presented in table 6.

There is no analytical formulae connecting the parameters θ^* and M_E for the axisymmetric geometry, contrary for the case 2D, the relation $\theta^*=\nu_E/2$ is checked [2] and [17], where ν_E presents the value of the Prandtl Meyer function corresponding to the exit Mach number M_E. It is noticed that the value of θ^* of the axisymmetric case is lower than the θ^* of the case 2D.

$$\theta^*_{axisymmetric} < \frac{\theta^*_{two-dimensional}}{2} \tag{83}$$

Figure 20 represents the variation of the Mach number through the wall of the nozzle. This figure shows the increase in the Mach number which is interpreted by the gas expansion. Between figures 20 and 18, the increase in the Mach number gives a decrease in pressure. The intersection of the four curves of the figure 20 with the vertical axis gives the values of M^*. In this point, there is an abrupt variation from M=1 to $M=M^*$ just after the throat. The values of M^* for the axisymmetric case are lower than the values for the case 2D.

On the figure 21, one notices a constant portion of the four curves. This portion indicates a uniform region BE of the figure 1. The other portion indicates the variation of the Mach number on the axis of symmetry in the Kernel region, of M=1 to $M=M_E$ (M_E=3.00 for our example). The length of Kernel is different for the four curves.

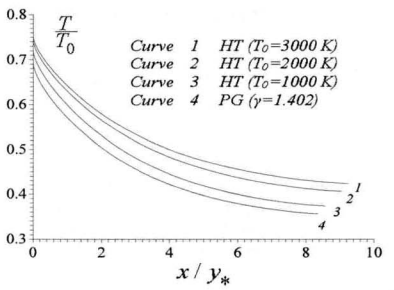

Fig. 16. Variation of T/T_0 along the wall for M_E=3.00

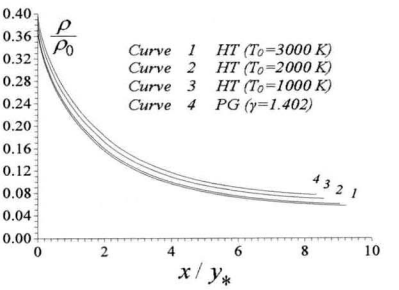

Fig. 17. Variation of ρ/ρ_0 along the wall for M_E=3.00

Table 5. Position of the deflection point

	γ=1.402		T_0=1000K		T_0=2000K		T_0=3000K	
M_E	x/y_*	y/y_*	x/y_*	y/y_*	x/y_*	y/y_*	x/y_*	y/y_*
1.5	0.43	1.02	0.43	1.02	0.43	1.02	0.43	1.02
2.0	0.56	1.07	0.57	1.08	0.57	1.08	0.57	1.08
3.0	0.70	1.18	0.71	1.19	0.72	1.21	0.73	1.21
4.0	0.81	1.28	0.82	1.29	0.84	1.32	0.85	1.34
5.0	0.88	1.38	0.89	1.38	0.89	1.41	0.90	1.43
6.0	0.91	1.44	0.92	1.44	0.92	1.47	0.93	1.50

Table 6. Values of M and θ in deflection point

	γ=1.402		T_0=1000K		T_0=2000K		T_0=3000K	
M_E	M	θ (°)	M	θ (°)	M	θ (°)	M	θ (°)
1.5	1.27	3.75	1.27	3.91	1.27	4.01	1.27	4.05
2.0	1.50	8.28	1.50	8.66	1.50	9.00	1.51	9.11
3.0	1.84	15.44	1.84	16.10	1.86	17.09	1.87	17.46
4.0	2.07	20.25	2.07	20.95	2.10	22.38	2.12	23.10
5.0	2.23	23.55	2.24	24.22	2.26	25.79	2.28	26.79
6.0	2.35	25.87	2.36	26.54	2.37	28.13	2.40	29.25

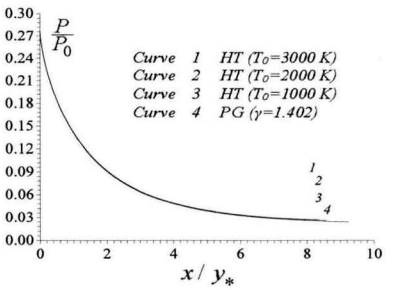

Fig. 18. Variation of P/P_0 along the wall for M_E=3.00

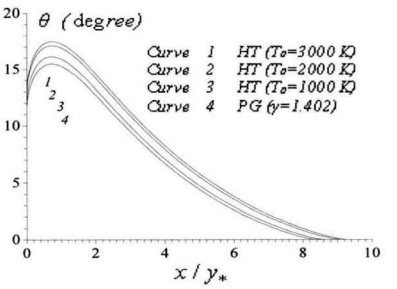

Fig. 19. Variation of θ^* along the wall for M_E=3.00

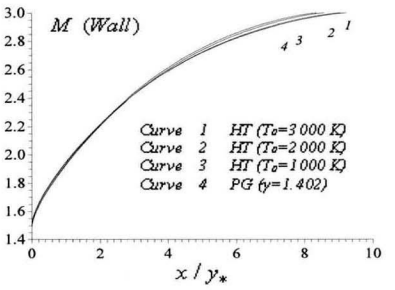

Fig. 20. Variation of M along the wall for M_E=3.00

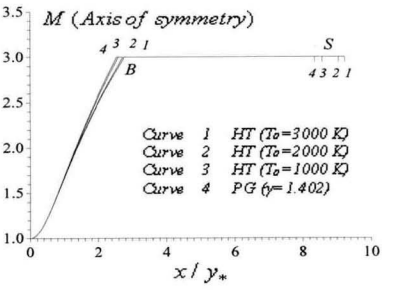

Fig. 21. Variation of M along the axis of symmetry for M_E=3.00

Figures 20 and 21 shows the flow is axis of symmetric. For a given section, the Mach number decreases according to the ray of the nozzle. For example, when T_0=3000K and x/y_*=2.00, there will be approximately M=2.56 on the axis of symmetry and M=2.21 on the wall.

5.4. Variation of the design parameters according to the exit Mach number

Figures 22 to 29 represent the required variation at high temperature of the design parameters of the nozzle to have a uniform and parallel flow at the exit section. It is clear that T_0 influences all the design parameters and that the more its value is raised, the more the difference between the two models increases, which gives the need for taking into account of T_0. The curves 3 and 4 of each figure representing respectively the results of the HT model when T_0=1000K and for the PG model (γ=1.402). One notices that the four curves are almost confounded until Mach number M_E=2.00, then starts progressively to differentiate with M_E and T_0. This result is interpreted by the use potential of the PG model to design the supersonic nozzles as long as M_E either lower than 2.00 independently of T_0, or if T_0<1000K independently of M_E.

On figure 22 shows that the more the nozzle delivers a raised exit Mach number, the more the nozzle becomes open to the throat to allow an adapted suitable expansion, in order to give a uniform and parallel flow. In the same way, for a given Mach number, even T_0 increases, the nozzle must be opened at the throat.

Figure 23 shows the existence of a deflection point on the wall of the nozzle in the vicinity of the throat having a value θ_{max} near to θ^*, which is not the case for the geometry 2D. For some values of M_E and T_0, the position, as well as the Mach number at the points of deflection is presented in the tables 5 and 6.

Figure 24 determines the Mach number M^* just after the expansion (at point A) of the throat necessary to give a uniform and parallel flow at the exit. This Mach number represents the value at the first point of last C^- of zone of Kernel.

Figure 25 gives the variation at high temperature of the length of Kernel versus M_E. The more the nozzle delivers a raised exit Mach number, the more the length L_d becomes large. The goal of the presentation of this figure is that one can directly deduce the length of the nozzle without making the flow calculation in the zone of transition, considering the flow in the zone BSE is uniform and parallel.

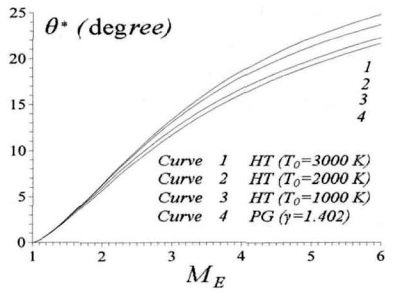

Fig. 22. Variation of the angle θ^* versus M_E

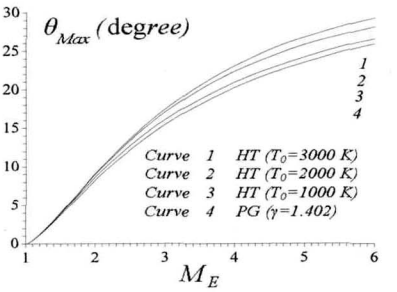

Fig. 23. Variation of the angle θ_{max} versus M_E

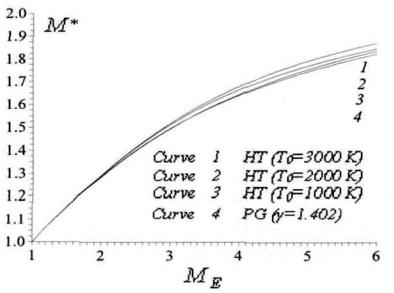

Fig. 24. Variation of M^* versus M_E

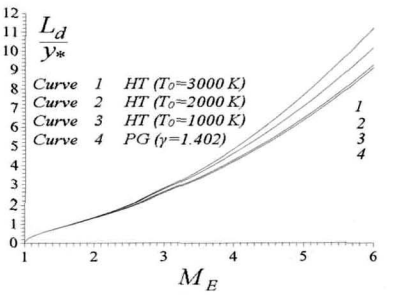

Fig. 25. Variation of L_d versus M_E

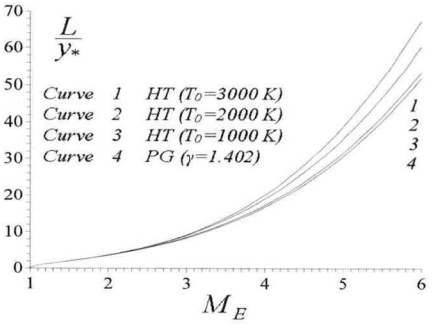

Fig. 26. Variation of L versus M_E

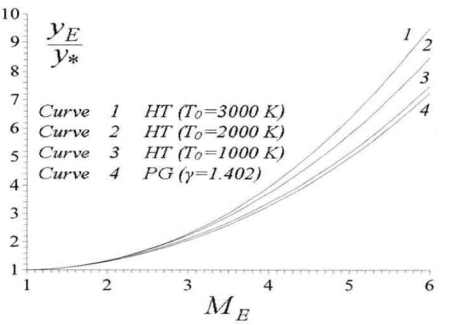

Fig. 27. Variation of the exit section ray versus M_E

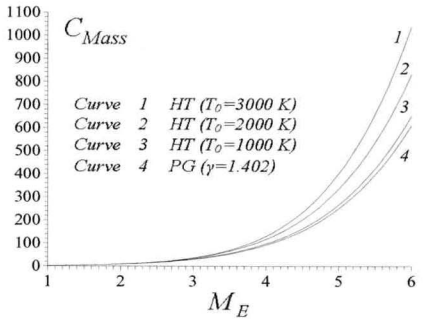

Fig. 28. Variation of C_{mass} versus M_E

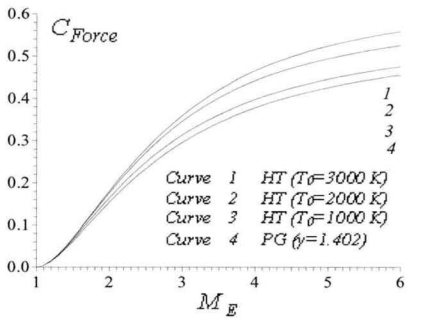

Fig. 29. Variation of C_{Force} versus M_E

The length of the nozzle presented in figure 26 is connected with the length of Kernel by the relation (84). The critical cross sectional ratio in this relation must be calculated by the formulae (67).

$$\frac{L}{y_*}=\frac{L_d}{y_*}+\frac{A_E}{A_*}\sqrt{M_E^2-1} \tag{84}$$

Figure 27 represents the variation of the exit section ray. The value of the ray is that obtained by numerical calculation using the relationship (64) with an error better with 10^{-4}.

One can plot the curves of this figure independently of the design calculation (flow 1D). It is enough to determine the value of T_E corresponding to M_E, and T_* corresponding to T_0, then to integrate the function $F_A(T)$ using the relation (67), to obtain the ray of the exit section.

Figures 28 and 29 present respectively the variation, in non-dimensional form, of the mass of the nozzle and the pressure force exerted on the wall, necessary to obtain a uniform and parallel flow at the nozzle exit.

5.5. Variation of the design parameters according to the stagnation temperature

Figures 30 to 37 present the variation of the various design parameters according to T_0 when M_E=3.00, for aim to make a comparison between the two models. The PG model is presented by a horizontal line, considering that does not depend on T_0. The HT model depends primarily on T_0. It is noticed that if T_0<240K, the HT model does not give no correction to the PG model, where ε=0.0. The more T_0 increases, the more the difference between the two models increases, and becomes considerable starting from T_0>1000K. If T_0<1000K, the variation for all parameters does not exceed 5%. If one draw the figures 30 to 37 for other values of M_E, the difference between the two models decreases if M_E decreases and increases if M_E increases.

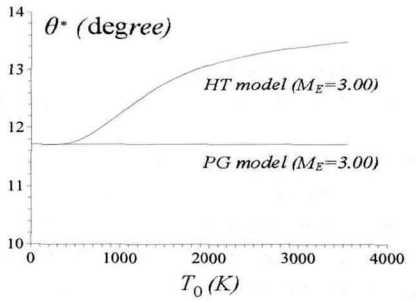

Fig. 30. Variation of the length of the nozzle versus T_0

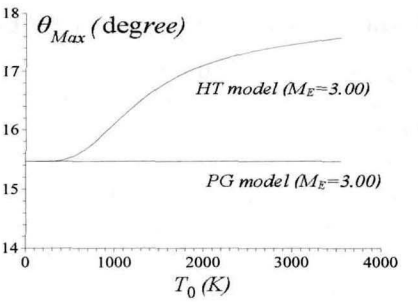

Fig. 31. Variation of the angle θ_{max} versus T_0

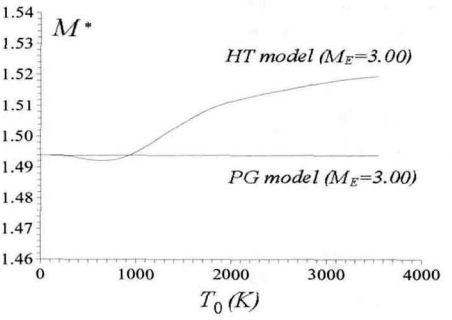

Fig. 32. Variation of M^* versus T_0

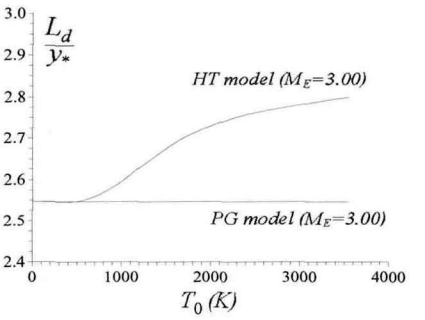

Fig. 33. Variation of L_d versus T_0

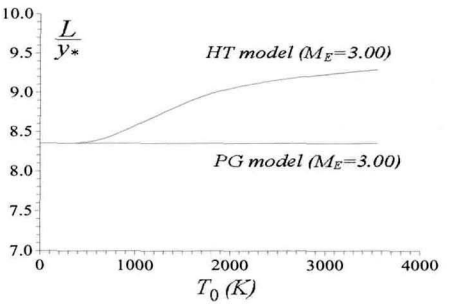

Fig. 34. Variation of L versus T_0.

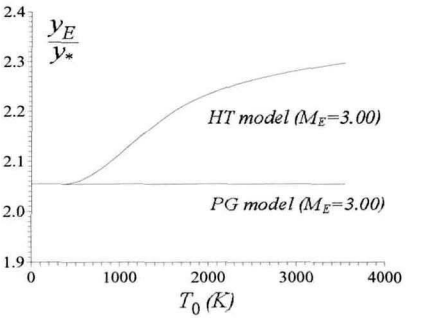

Fig. 35. Variation of the exit section ray versus T_0

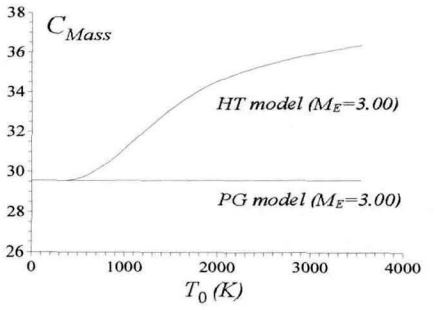

Fig. 36. Variation of C_{mass} versus T_0

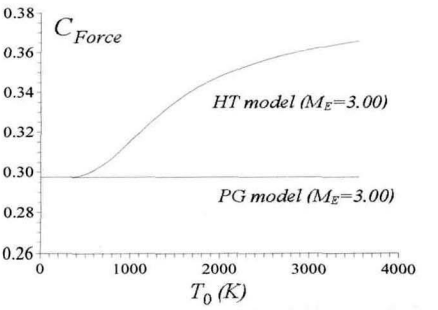

Fig. 37. Variation of C_{Force} versus T_0

5.6. Results on the error of the perfect gas model

Figure 38 shows the variation of the relative error given respectively by the length of the nozzle, the mass of the structure and the pressure force of the PG model compared to the HT model for some values of T_0.

It is clearly noticed that the error depends on the values of T_0 and M_E, and it increases if T_0 increases. For example, if T_0=2000K and M_E=2.50, the use of the PG model gives a relative error equal to ε=10 % for the length, ε=5 % for the mass of the structure and ε =13 % for the pressure force. One can notice that with low value of M_E and T_0, the error ε is small. On these figures, the curve 3 is lower part of the error 5%. This position is interpreted by the use potential the PG model until T_0=1000K for the aeronautical applications. But if T_0 is raised, the error progressively increases and in this case, one can use the PG model independently of T_0, if the Mach number does not exceed M_E=2.00.

The relative error given when M=1 (intersection of the curves with the vertical axis of the error) can be obtained for each parameters by using the relations (85), (86) and (87). The removal of the non-determination in the relation (86) is made by the use of the relation (76). For the pressure force, one uses the relation (79).

$$\varepsilon_{(L/y_*)}(M=1)=\lim_{\substack{M\to 1\\ T\to T_*}}\left|1-\frac{(L/y_*)_{PG}(M)}{(L/y_*)_{HT}(T)}\right|\times 100=0 \tag{85}$$

$$\varepsilon_{(C_{Mass})}(M=1)=\lim_{\substack{M\to 1\\ T\to T_*}}\left|1-\frac{(C_{Masse})_{PG}(M)}{(C_{Masse})_{HT}(T)}\right|\times 100=0 \tag{86}$$

$$\varepsilon_{(C_{Force})}(M=1)=\lim_{\substack{M\to 1\\ T\to T_*}}\left|1-\frac{(C_{Force})_{PG}(M)}{(C_{Force})_{HT}(T)}\right|\times 100= \tag{87}$$

$$\left|1-\frac{0}{0}\right|\times 100=\begin{cases}4.724\ \%\ \text{pour}\ T_0=1000\ \text{K}\\ 7.474\ \%\ \text{pour}\ T_0=2000\ \text{K}\\ 8.368\ \%\ \text{pour}\ T_0=3000\ \text{K}\end{cases}$$

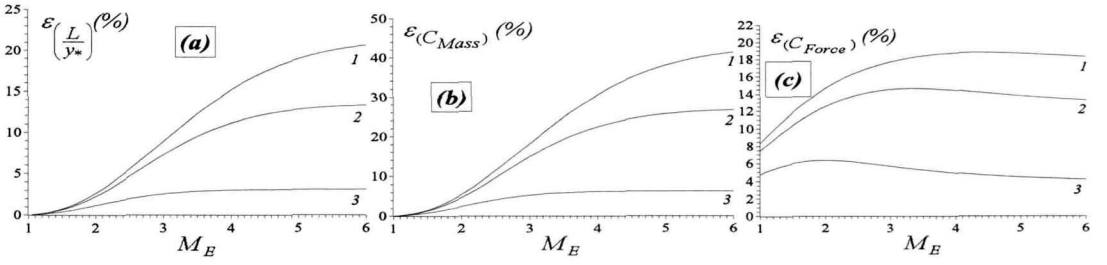

Curve 1 Error compared to HT model when (T_0=3000K)
Curve 2 Error compared to HT model when (T_0=2000K)
Curve 3 Error compared to HT model when (T_0=1000K)

Fig. 38. Variation of the relative error given by the design parameters of the PG model versus M_E
(a): Length (b) : Mass (c) : Pressure force

5.7. Various results

Figures 39 and 40 present respectively the iso-Mach and the iso-direction curves.

The obtained curves in the region of transition are not of straight lines, considering this zone is non-simple waves, contrary to the case 2D, where one found straight line segments, to see reference [17]. These figures show that the flow is axisymmetric with a uniform and parallel flow at the exit section.

In the figure 40, the curves cut the wall of the nozzle in two points, which shows the existence of the deflection point having $\theta = \theta_{max}$. It is noticed that some of the iso-value curves pass by point A of the throat, which indicates that the iso-Mach curves have a Mach number $M \leq M^*$ and the iso-direction curves have $\theta \leq \theta^*$. The points having a $\theta = 0$ (null direction) are the points of the throat, the axis of symmetry and all points in the triangular uniform region.

Figure 41 present the forms of four nozzles having even exit section ray. Curves 1, 2 and 3 are for HT model respectively when T_0=3000K, 2000K and 1000K. Curve 4 correspondents to the PG model. The four nozzles having an exit section ray of the PG case for M_E=3.00. It is equal to $y_E / y_* = 2.054$. One can show that they do not deliver the same Mach number M_E starting from the relations (4) and (67). The goal to present this figure is that, if one considers the designed nozzles on the basis of PG model for the aeronautical applications, one can notice the degradation of the performances in particular the exit Mach number, considering the nozzles have almost the same size and form, except a small difference in length. The numerical results of the principal parameters are presented in the table 7. The flow in this difference in length is almost uniform. The shape of the used nozzle does not change, except the thermodynamic behaviour of air with the temperature.

Table 7. Numerical values of de nozzle design of the figure 41

	M_E	θ^* (°)	M^*	$\frac{L}{y_*}$	C_{Mass}	C_{Force}
γ=1.402	3.00	11.71	1.49	8.35	29.56	0.29
T_0=1000K	2.94	11.92	1.48	8.18	28.99	0.30
T_0=2000K	2.84	12.13	1.48	7.94	28.10	0.32
T_0=3000K	2.81	12.20	1.48	7.87	27.83	0.33

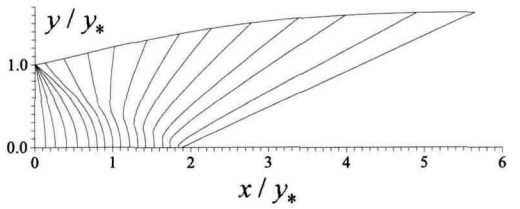

Fig. 39. Iso-Mach curves

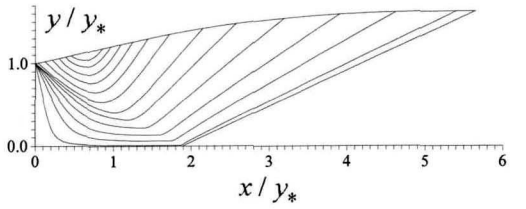

Fig. 40. Iso-direction curves

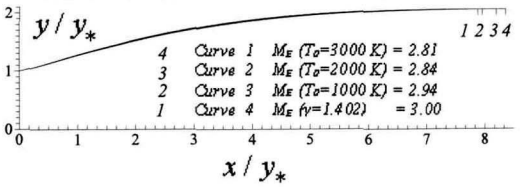

Fig. 41. Nozzles having same exit section ratio giving M_E=3.00 for the PG model

6. Comparison between the 2D and axisymmetric nozzles

Figure 42 presents the shapes of the 2D and axisymmetric nozzles, giving M_E=3.00 for T_0=2000K. The two nozzles have even exit section ray. The non-dimensional exit section ray is equal to the exit section ratio for the case 2D and equal to the square root of the exit section ratio for the axisymmetric case.

The produced pressure force of the nozzle is the same one for the two geometries.

For the mass of the nozzle, in really, one cannot make in this form a comparison of this parameter, considering that, one did not add the mass of both vertical left and right for the case 2D. They are an infinitum (does not exist).

The 2D nozzle is opened at the throat compared to the axisymmetric one. The obtained values of θ^* checked the relation (83).

A comparison for some design parameters is made in figure 43. The length of the axisymmetric nozzle is approximately equal to the square root of the length of the 2D nozzle.

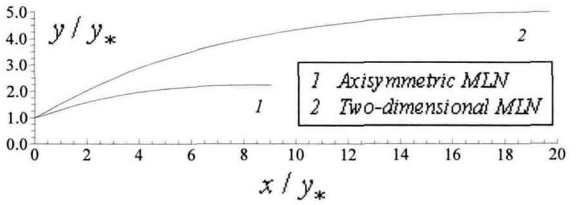

Fig. 42. Two-dimensional and axisymmetric nozzles giving M_E=3.00 for T_0 =2000K

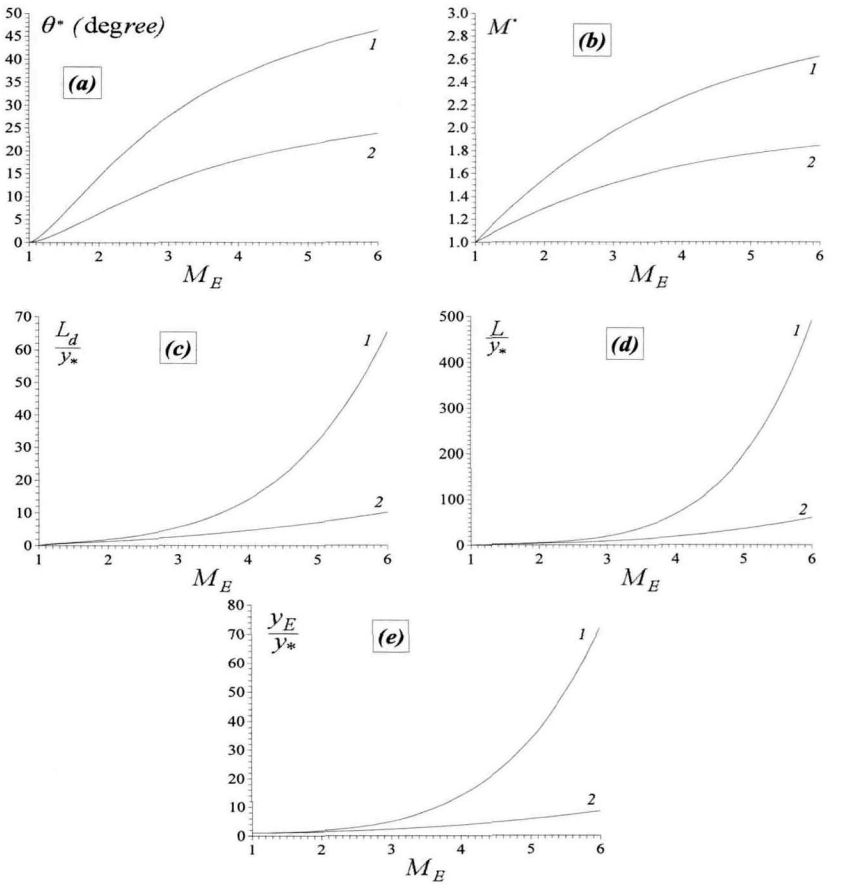

Curve 1 Two-dimensional MLN
Curve 2 Axisymmetric MLN

Fig. 43. Comparison of the design parameters according to M_E between the 2D and axisymmetric geometries when T_0=2000K
(a) : Angle θ^* (b) : Mach number M^* (c) : Length of Kernel
(d) : Length of nozzle (e) : Exit section ray

Conclusion

If an error lower than 5% is accepted, one can study a supersonic flow by using the PG relations, if the stagnation temperature is lower than 1000 K for any value of the Mach number, or when the Mach number is lower than 2.00 for any stagnation temperature up to approximately 3000 K.

The basic variable for our model is the temperature and for model PG model is the Mach number, because of a nonlinear implicit equation connecting these two parameters.

The presented relations are valid for any interpolation chosen for the function $C_P(T)$. The essential one is that the selected interpolation gives an acceptable small error. One can choose of another substance instead of air. The relations remain valid, except that it is necessary to have the table of variation of $C_P(T)$ according to the temperature, and to make a good interpolation. The ratio of the theoretical sections can be used like *a source of comparison for the validation of the numerical results design of the various supersonic nozzles giving* a uniform and parallel flow at the exit section by the method of characteristics.

One can obtain the perfect gas relations starting from the relations of the HT model by cancelling all constants of interpolations of the function $C_P(T)$ except the first. In this case, the *PG* model becomes a particular case of our HT model. For low temperature and Mach number, the difference in results between the two models is small, which gives the possibility of studying a HT flow by using the PG model relations. The axisymmetric nozzle has a point of deflection.

The determination of the parameters in the flow fields' points by the use of the predictor corrector algorithm requires iterations in more for HT model compared to the PG model for same precision. The difference between the numbers of iteration count is approximately 30%, which influence over the numerical computing time. The results of design by the method of characteristics depend primarily on the upstream results, independently of the downstream results. A bad provision of the points at the throat can' t give a quickly convergence of calculations towards the desired solution. The use of the PG model for the supersonic nozzle design degrades the real performances of the design parameters, in particular the Mach number and the pressure force, if the combustion chamber temperature T_0 is high.

The conservation of the determined design parameters by the PG model requires a change of the shape of the nozzle which supports these parameters.

The expansion in a axisymmetric nozzle is faster compared to that in the 2D nozzle.

One proves the existence of the infinity of profiles having same exit Mach number, by changing the stagnation temperature.

Acknowledgments

The author acknowledges Fettoum MEBREK and Djamel, Khaoula, AbdelGhani Amine ZEBBICHE for granting time to prepare this manuscript.

References

1. Anderson J. D. Jr., "Fundamentals of Aerodynamics," Mc Graw-Hill Book Company, New York, 1982.

2. Anderson J. D. Jr., "Modern Compressible Flow: With Historical Perspective," Mc Graw-Hill Book Company, New York, 1988.

3. Argrow B. M. and Emanuel G., "Comparison of Minimum Length Nozzlesn," J. Fluid Eng. September, Vol. 110, PP. 283-288, 1988.

5. Demidovitch B. and Maron I., "Eléments de calcul numérique, " Edition MIR, Moscou, 1987.

6. Dumitrescu L. Z., "Minimum Length Axisymmetric Laval Nozzles," AIAA J. 13, 520-532, 1975.

7. Emanuel G., "Gasdynamic: Theory and Application" , New York, AIAA Educational Serie, 1986.

8. Fletcher C. A. J., " Computational Techniques for Fluid Dynamics: Specific Techniques for Different Flow Categories," Vol. II, Springer Verlag, Berlin, Heidelberg, 1988.

9. Oosthuisen P. H. and Carscallen W. F., "Compressible Fluid Flow," Mc Graw-Hill, New York, 1997.

10. Peterson C. R. and Hill P. G., "Mechanics and Thermodynamics of Propulsion," Addition-Wesley Publishing Company Inc, 1965.

11. Raltson A. and Rabinowitz A., "A First Course in Numerical Analysis," McGraw Hill Book Company, 1985.

12. Rao G. V. R., "Contoured Rocket Nozzles," Proc. 9Th Int. Astro-Fed. Congress, Amsterdam, 1958.

13. McLain D. H., "Drawing contours from arbitrary data points," The Computer Journal, Vol. 17, PP. 318-324, 1974.

14. Zebbiche T. and Youbi Z., "Fonction de Prandtl Meyer à Haute température, " Conférences Internationales de la Mécanique Avancée, Boumerdes, Algérie, 30 Nov.-02 Dec. 2004.

15. Zebbiche T. and Youbi Z., "Supersonic Flow Parameters at High Temperature. Application for Air in Nozzles," DGLR-2005-256. German Aerospace Congress 2005, 26-29 Sep. 2005, Friendrichshafen, Germany.

16. Zebbiche T. and Youbi Z., "Supersonic Plug Nozzle Design at High Temperature. Application for Air," AIAA Paper 2006-0592, 44th Aerospace Sciences Metting and Exhibit, 9-12 Jan. 2006, Reno Nevada, Reno Hilton, USA.

17. Zebbiche T. and Youbi Z., "Design of Two-Dimensional Supersonic Minimum Length Nozzle at Higth Temperature. Application for Air," DGLR 2005-257. German Aerospace Congress 2005, 26-29 Sep. 2005, Friendrichshafen, Germany.

18. Zebbiche T., "New Generalized Form of the Prandtl Meyer Function. Application for Air at High Temperature," AIAA-2006-3674, 25th Applied Aerodynamics Conference, San Francisco, California, 5-8 Jun 2006.

19. Zucker R. D. and Bilbarz O., "Fundamentals of Gasdynamics, " John Wiley & Sons., New York 2002.

20. Zucro M. J. and Hoffman J. D., "Gas Dynamics," Vol. 1, Vol. 2, New York, Wiley, 1976.

21. Zebbiche, T., "Stagnation Temperature Effect on the Prandtl Meyer Function," *AIAA Journal*, Vol. 45, No. 4, 2007, pp. 952-954.

22. Zebbiche, T. and Youbi, Z., "Effect of Stagnation Temperature on the Supersonic Flow Parameters with Application for Air in Nozzles," KSAS International Journal, Vol., 7, N° 1, May 2006, pp.13-26.